

DOI: 10.12442/j.issn.1002-185X.20240716

# Microstructure homogenization control of GH4706 alloy using hot deformation maps

Zheng Deyu, Xia Yufeng, Zhou Jie

Chongqing Key Laboratory of Advanced Mold Intelligent Manufacturing, School of Material Science and Engineering, Chongqing University, Chongqing 400044, China

**Abstract:** Hot compression tests for GH4706 alloy were performed at a true strain of 1.2 within a temperature range of 950-1150 °C and a strain rate range of 0.001-1 s<sup>-1</sup>. The optimal hot deformation temperature and strain rate range were determined using nephogram maps for dynamic recrystallization (DRX) fraction, average grain size, and grain distribution standard deviation. Processing maps at true strains from 0.4 to 0.9 were generated based on flow stress curves to identify the strain corresponding to optimal microstructure homogenization efficiency at various temperatures and strain rates. Within the optimal parameter range, processing maps indicated that the true strain of 0.6 was the optimal microstructure homogenization efficiency at 1150 °C and 0.01 s<sup>-1</sup>. The grain orientation spread (GOS) maps obtained from the experiment confirmed this conclusion. This study provides an effective method for microstructure homogenization control of GH4706 alloy. Meanwhile, it can provide effective reference for the minimum strain threshold of the local part of the forging in engineering.

**Key words:** GH4706 alloy; dynamic recrystallization; microstructure; homogenization efficiency; processing map

GH4706 (IN706) is a typical Ni-Fe-Cr alloy with excellent cold and hot formability. Its creep resistance and oxidation resistance make it a fundamental material for hot segment aero-engine components, such as turbine disks, blades and shells<sup>[1-3]</sup>. The microstructure of alloy should be homogeneous and refine to ensure the service life of forgings in the extreme environment of aviation and nuclear industry<sup>[4]</sup>. To achieve this goal, a much homogenic grain structure must be obtained through the dynamic recrystallization (DRX) process during hot deformation<sup>[5]</sup>. However, the flow behavior of GH4706 with the corresponding microstructure development is very sensitive to processing parameters such as strain, temperature and strain rate, which constrains the suitable processing parameters in narrow hot working windows<sup>[6]</sup>. Especially for the super large forgings using expensive nickel base alloys<sup>[7]</sup>, the cost of a traditional trial-and-error method for the identification of processing parameters is unacceptable. Therefore, it is necessary to find an effective method to optimize the microstructure of GH4706 alloy.

It is widely accepted that hot deformation maps which con-

tains nephogram and processing map are valuable for identifying the optimal processing parameters across a wide range of strains, strain rates and temperatures<sup>[6-9]</sup>. Prasad et al.<sup>[10]</sup> developed the processing map based on the dynamic material model (DMM). According to DMM theory, the power dissipation efficiency ( $\eta$ ) is calculated from the distribution of strain rate sensitivity ( $m$ ) with deformation temperature and strain rate, which characterizes the metallurgical mechanism distribution at a given temperature and strain. To date, the hot processing map has been widely used to determine the favorable hot working parameters and regulating the corresponding microstructure<sup>[11]</sup>. Huang et al.<sup>[6]</sup> developed the hot deformation maps of hot working parameters for GH4706 alloy at true strain of 0.7, 900-1150 °C temperature and 0.001-1 s<sup>-1</sup> strain rate, identifying optimal hot working conditions of 940-970 °C and 0.015-0.003 s<sup>-1</sup>, which laid the groundwork for future material applications. However, with increasing size and performance requirements for GH4706 alloy forgings, it is essential to further refine the optimal parameters window for super large forgings.

Received date:

Foundation item: National Key R&D Program Project Topic (2022YFB3705103).

Corresponding author: Xia Yufeng, PH. D., Professor, School of Material Science and Engineering, Chongqing University, Chongqing 400044, P. R. China, Email: [yufengxia@cqu.edu.cn](mailto:yufengxia@cqu.edu.cn).

Copyright © 2019, Northwest Institute for Nonferrous Metal Research. Published by Science Press. All rights reserved.

Most people agree that DRX nucleation is more favorable the higher the strain. This is due to the fact that as strain increases, so does the dislocation density and stored energy<sup>[12]</sup>. Though the degree of DRX rises with strain, DMM theory<sup>[10]</sup> demonstrates that the power efficiency of microstructure rebuilding should be taken into account. This is fully confirmed by the typical nonlinear relationship between DRX evolution and strain<sup>[13]</sup>. Additionally, Quan et al. <sup>[8]</sup> demonstrates that when strain increases during hot deformation, the area of the ideal process window first grows and subsequently declines. This indicates that there is DRX efficiency inflection point as the strain increases. Thus, it is imperative to take into account the impact of strain on DRX efficiency which was called microstructure homogenization efficiency in this text.

The purpose of this study is to identify the ideal range for hot deformation temperature and strain rate using nephogram maps of DRX results. It also aims to identify the optimal strain, which is defined as the strain with optimal microstructure homogenization efficiency corresponds to various temperatures and strain rates, by drawing processing maps of the GH4706 alloy at various strains based on flow stress curves. This study will provide an effective method for microstructure homogenization control of GH4706 alloy. Meanwhile, it will provide effective reference for the minimum strain threshold of the local part of the forging in engineering.

## 1 Experiment

The material used in this study is forged GH4706 alloy, whose isothermal hot compression tests were carried out on a computer-controlled hydraulic Gleeble-1500 thermal simulator. The samples were cut into a diameter of 8 mm and a height of 15 mm by wire-electrode cutting. To reduce the anisotropy of flow behavior, each sample was heated to the deformation temperature at a heating rate of 10 °C/s and maintained for 180 seconds. The deformation temperature range was 950-1150 °C with the increment of 50 °C, and the strain rate were 0.001, 0.01, 0.1 and 1 s<sup>-1</sup>, respectively. Following the compression test to the true strain of 1.2, the samples were quenched in water immediately. In addition, six additional samples were compressed at 1150 °C / 0.01 s<sup>-1</sup> under 0.4-0.9 strains to verify the optimal strain. The true stress and true strain curves were automatically recorded. The electron backscatter diffraction (EBSD) observations were carried out in the middle area of cutting samples under JSM 7800F scanning electron microscope. The EBSD samples were ground to 3000# with silicon carbide sandpaper, and were electro-polished in an electrolyte solution of 10% HClO<sub>4</sub> and 90% C<sub>2</sub>H<sub>5</sub>OH at 22 V for 20 s. The prepared samples were stored in alcohol solution. Fig. 1 shows the initial microstructure of forged GH4706 alloy.

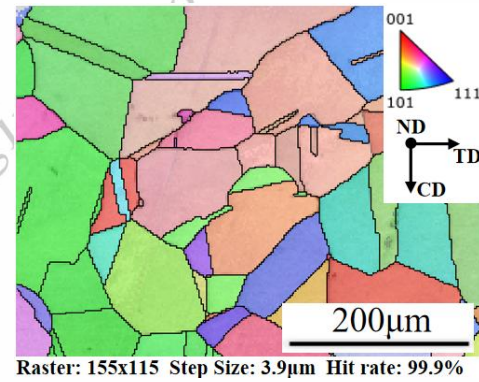


Fig. 1 Initial microstructure of GH4706 alloy

## 2 Computing Method

### 2.1 Processing map theory

Based on the dynamic material model (DMM) <sup>[10]</sup>, the total power consumption  $P$  of the material during compression is related to the flow stress and strain rate, including two complementary parts. The first part is the power consumption  $G$  due to temperature rise; The second part is the power consumption  $J$  of microstructure evolution. The relationship between them can be expressed as equation (1):

$$P = \sigma \dot{\epsilon} = \int_0^{\dot{\epsilon}} \sigma d\dot{\epsilon} + \int_0^{\sigma} \dot{\epsilon} d\sigma = G + J \quad (1)$$

Where  $\sigma$  is the stress and  $\dot{\epsilon}$  is the strain rate. The ratio  $m$  between  $G$  and  $J$  reflects the sensitivity of stress to strain rate at a certain temperature  $T$  and a certain strain  $\epsilon$ , which can be expressed as equation (2):

$$m = \left. \frac{\partial J}{\partial G} \right|_{T, \epsilon} = \frac{\partial J}{\partial P} \frac{\partial P}{\partial G} = \frac{\sigma d\dot{\epsilon}}{\dot{\epsilon} d\sigma} = \left. \frac{\partial \ln \sigma}{\partial \ln \dot{\epsilon}} \right|_{T, \epsilon} \quad (2)$$

The relationship between stress and strain rate can be expressed in the power law form of  $m$  (3):

$$\sigma = K \dot{\epsilon}^m \quad (3)$$

Where  $K$  is the undetermined constant. By substituting equation (3) into equation (1), the expressions (4) and (5) of  $J$  and  $G$  are obtained respectively:

$$J = \frac{m\sigma\dot{\epsilon}}{m+1} \quad (4)$$

$$G = \frac{\sigma\dot{\epsilon}}{m+1} \quad (5)$$

The power dissipation efficiency of microstructure evolution,  $\eta$ , is the ratio of the actual dissipation  $J$  to the ideal dissipation  $J_{ideal}$  ( $J_{ideal} = 0.5\sigma\dot{\epsilon}$ ) when  $m=1$ , which is a function of  $m$  (6):

$$\eta = \frac{J}{J_{ideal}} = \frac{2m}{m+1} \quad (6)$$

To avoid the fluctuation of power dissipation parameters caused by material flow instability, it is specified that the ma-

material will flow instability when the entropy generation rate in the metallurgical system reaches the maximum. Based on this, the plastic flow instability equation<sup>[14]</sup> (7) is given as:

$$\frac{\partial \ln J}{\partial \ln \dot{\epsilon}} < 1 \quad (7)$$

The expression of  $\xi(\dot{\epsilon})$  can be obtained by substituting equation (4) into equation (7), and  $\xi(\dot{\epsilon}) < 0$  is defined as instability criterion (8):

$$\xi(\dot{\epsilon}) = \frac{\partial \ln \left( \frac{m}{m+1} \right)}{\partial \ln \dot{\epsilon}} + m < 0 \quad (8)$$

The ideal microstructure control is realized through the superposition of the power dissipation map and the instability map to establish the processing map.

## 2.2 Standard deviation of grain size distribution

The average grain size and DRX fraction response maps can reflect the quantitative relationship between microstructure and parameters intuitively<sup>[15]</sup>. However, it is not enough to reflect the distribution of grain size.

The standard deviation of grain size distribution  $S$  is used to express the fluctuation of grain size to further quantify the grain size distribution, as shown in equation (9):

$$S = \sqrt{\frac{\sum_{i=1}^n (x_i - \bar{x})^2}{n}} \quad (9)$$

Where  $n$  is the number of grains;  $x_i$  and  $\bar{x}$  are the diameter of the  $i$ -th grain diameter and the average grain diameter, respectively. The larger the  $S$  value, the greater the fluctuation of grain size; on the contrary, the smaller the  $S$  value, the more uniform the grain size distribution.

## 3 Experimental results and analysis

### 3.1 Flow stress curves

Fig. 2a-2d show the true stress-strain curves of GH4706 alloy under the deformation temperature range of 950-1150 °C and the strain rate range of 0.001-1 s<sup>-1</sup> when the specimens are compressed to the true strain of 1.2 (1.2 true strain is the average strain of a GH4706 alloy super large forging). It is evident that there is a substantial relationship between stress and temperature, strain rate, and strain. The stress increases with the increase of strain rate and with the decrease of temperature. The flow stress increases rapidly at small strain, then increases slowly with deformation, and finally tends to be stable. These are the macroscopic manifestations of microstructure evolution. DRX process includes two processes<sup>[16]</sup>: nucleation (interface formation) and growth (interface migration), which determine the grain refinement and coarsening, and the evolution shape of the stress-strain curve is determined by the competitive game relationship of them<sup>[17]</sup>.

### 3.2 Microstructure distribution at 1.2 strain

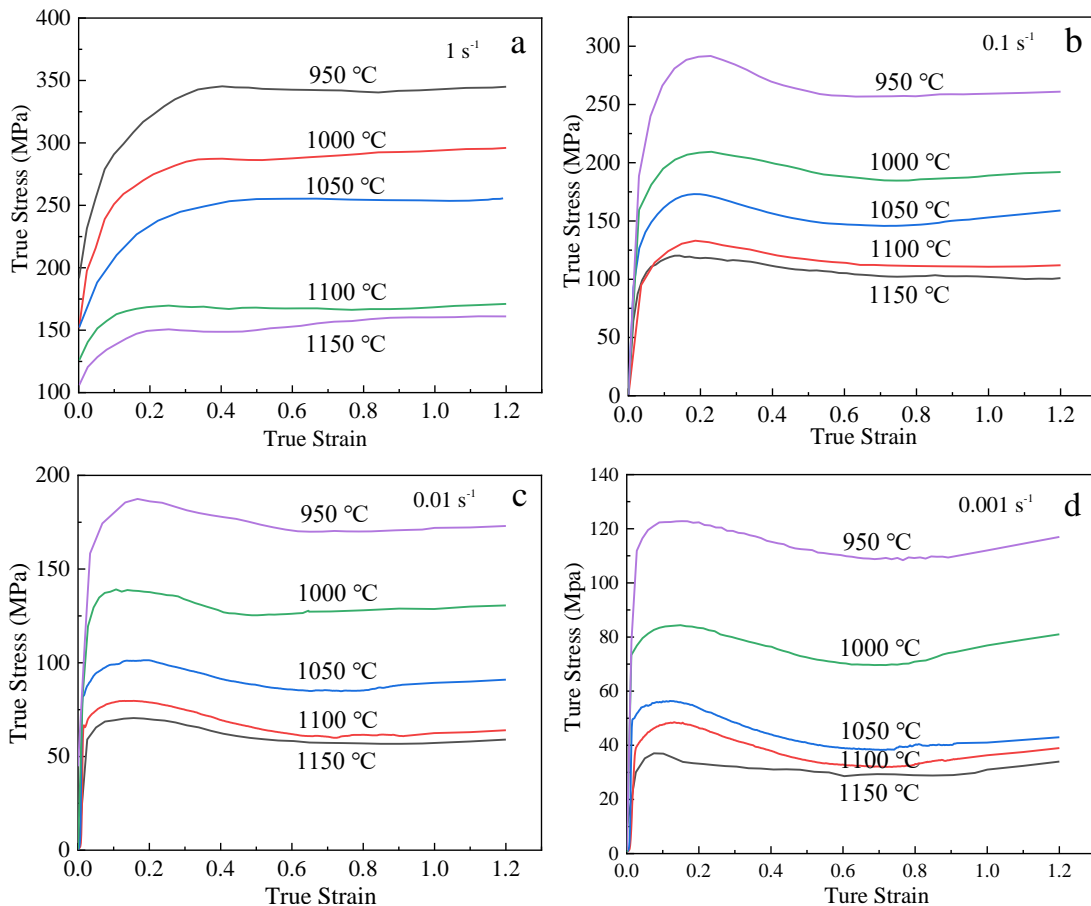


Fig. 2 Flow stress curves at different strain rates (a) 1 s<sup>-1</sup>, (b) 0.1 s<sup>-1</sup>, (c) 0.01 s<sup>-1</sup>, and (d) 0.001 s<sup>-1</sup>

Fig. 3a-3t show the microstructure maps of GH4706 alloy at a temperature range of 950-1150 °C and a strain rate range of 0.001-1 s<sup>-1</sup>, compressed to a strain of 1.2. It can be observed that the microstructure dominated by equiaxed grains (new DRX grains) is distributed below the red solid line A-A (high temperature and low strain rate), while the microstructure dominated by deformed grains (original grains) is distributed above the red solid line A-A (low temperature and high strain rate). Equiaxed grains below 1100 °C can only be obtained by reducing the strain rate to below 0.01 s<sup>-1</sup>, while above 1100 °C, they are easier to obtain and less affected by strain rate, as shown in Fig. 3s and 3t. However, excessive temperature and low strain rate can also promote grain growth, as shown in Fig. 3q and 3r. As temperature promotes grain boundary migration<sup>[15]</sup>, the microstructure exhibits strong work hardening or dynamic recovery characteristics as the temperature decreases. The strain rate promotes the nucleation of DRX, as the DRX process is mainly controlled by high nucleation at high strain rates<sup>[16]</sup>. Due to the short growth time of equiaxed grains, finer equiaxed grains will be obtained, as shown in Fig. 3h and 3l. Therefore, as the strain rate increases, there will be more equiaxed grains around the deformed grains, exhibiting a typical discontinuous DRX "necklace" microstructure. When the strain rate decreases, equiaxed grains will gradually replace the original deformed grains due to sufficient deformation time, as shown in Fig. 3e and 3i, indicating that lower strain

rates can accelerate the microstructure homogenization process.

### 3.3 The nephograms at 1.2 strain

Given the properties of GH4706 alloy, it is important to look into how DRX behavior responds to different process parameters in order to achieve the ideal homogenic equiaxed microstructure. The hot deformation map can reflect the relationship between hot deformation behavior and parameters<sup>[6]</sup>. The nephograms of DRX fraction, average grain size and grain distribution standard deviation at 1.2 true strain are shown in Fig. 4a-4c. We anticipate that the average grain size and the standard deviation of the grain distribution will decrease with increasing DRX fraction. The three response responses do not exhibit a straightforward monotonic relationship with temperature and strain rate, which highlights the intricacy of the DRX process. Average grain size decreases as a result of the progressive replacement of the original grains by newly generated DRX equiaxed grains during hot deformation. High temperatures will reduce grain boundaries and boost grain growth, both of which will raise average grain size. The extremely nonlinear growth of average grain size is determined by the game relationship of DRX evolution between grain coarsening and refinement<sup>[17]</sup>. Generally speaking, adequate DRX time at low or medium strain rates can yield the optimal microstructure. However, low strain rates and high temperatures will cause the grain to grow too quickly. While

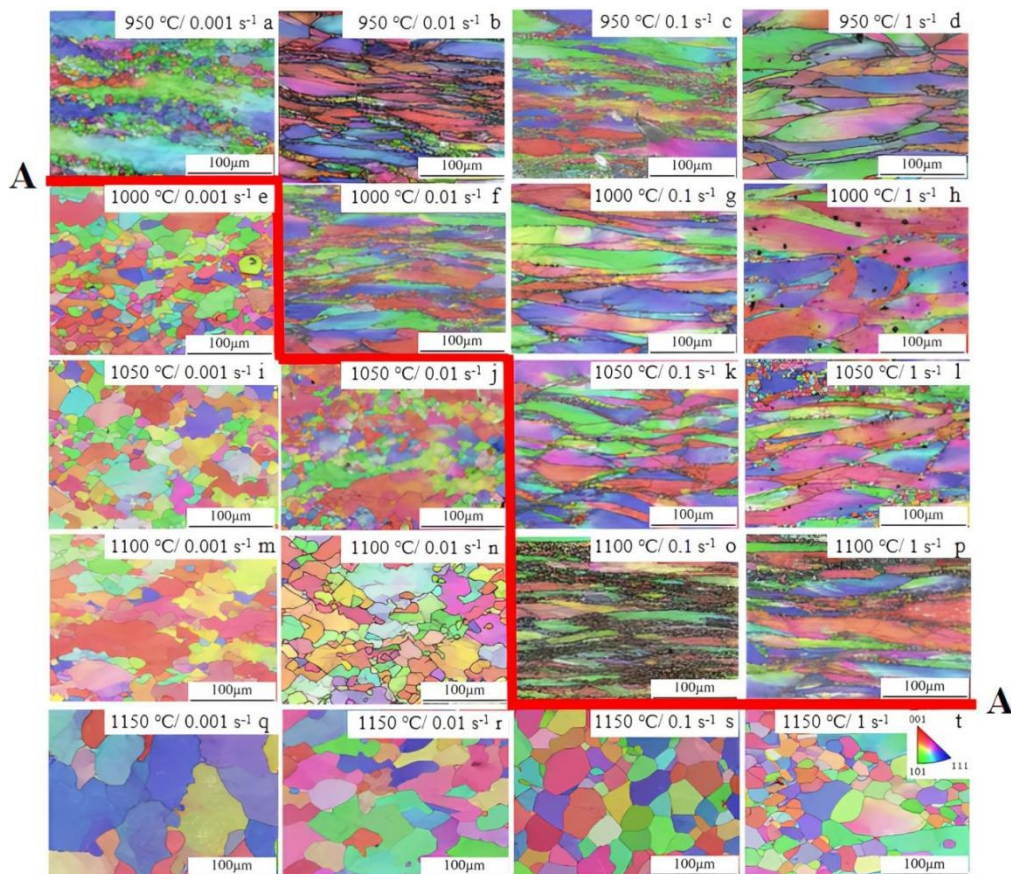


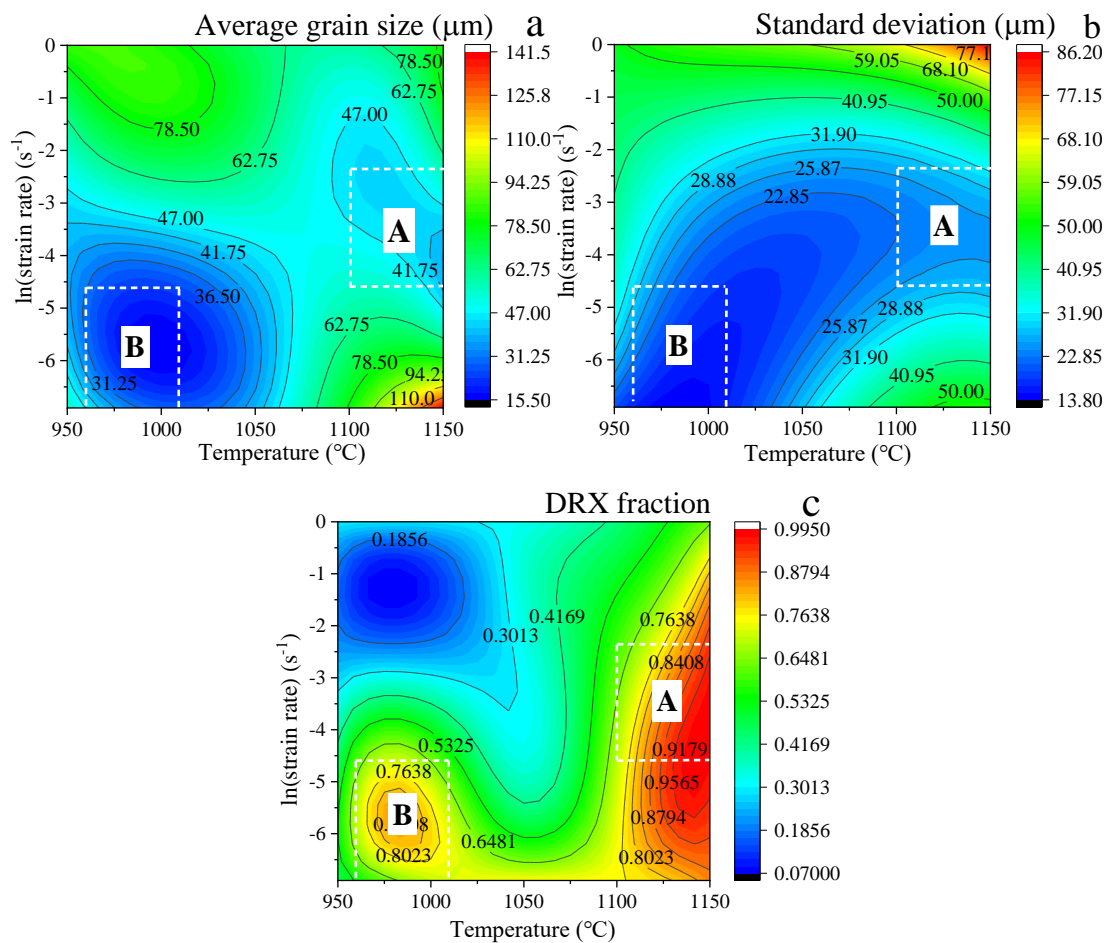
Fig. 3 Microstructure morphology at different temperatures and strain rates of GH4706 alloy (a-d) 950 °C, (e-h) 1000 °C, (i-l) 1050 °C, (m-p) 1100 °C, and (q-t) 1150 °C

an excessively low strain rate may cause the grain to expand and reduce production efficiency, an excessively high strain rate combined with an extremely low temperature would cause overload and damage to the equipment. Therefore, according to the comprehensive consideration of the three maps, and in combination with the forging load, two ideal parameters regions of A (1100-1150 °C / 0.01-0.1 s<sup>-1</sup>) and B (960-1010 °C / 0.001-0.01 s<sup>-1</sup>) are determined, which are similar to previous studies<sup>[6,7]</sup>.

### 3.4 Evolution of strain rate sensitivity response map with strain

The strain rate sensitivity  $m$  of flow stress reflects the sensi-

tivity level of flow stress to strain rate. It is a very important parameter to describe the macro behavior in the hot forming process, and also an important physical parameter to reflect the microstructure evolution mechanism<sup>[8-10]</sup>. Polynomial fitting was performed on the logarithm of stress and strain rate in order to obtain the true response of  $m$  to the parameters of strain, strain rate and temperature during hot deformation.  $m$  for each parameter was determined according to the slope of the corresponding point of the spline, as shown in Fig. 5a-5f.



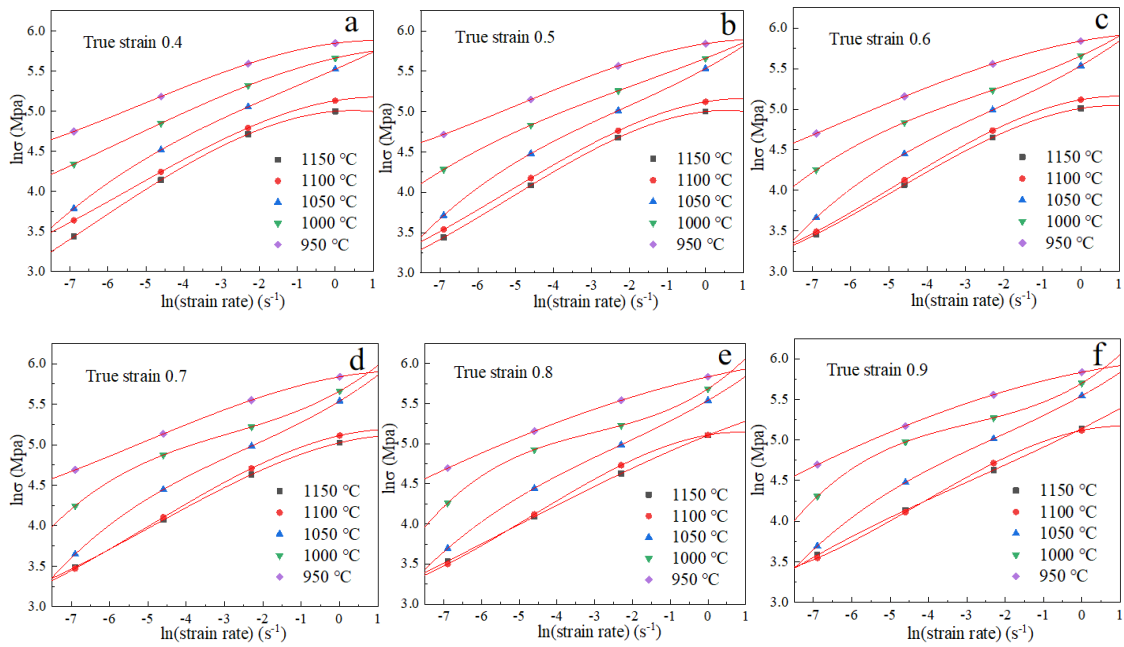


Fig. 5 The relationships between  $\ln\sigma$  and  $\ln(\text{strain rate})$  at different true strains of (a) 0.4, (b) 0.5, (c) 0.6, (d) 0.7, (e) 0.8, and (f) 0.9

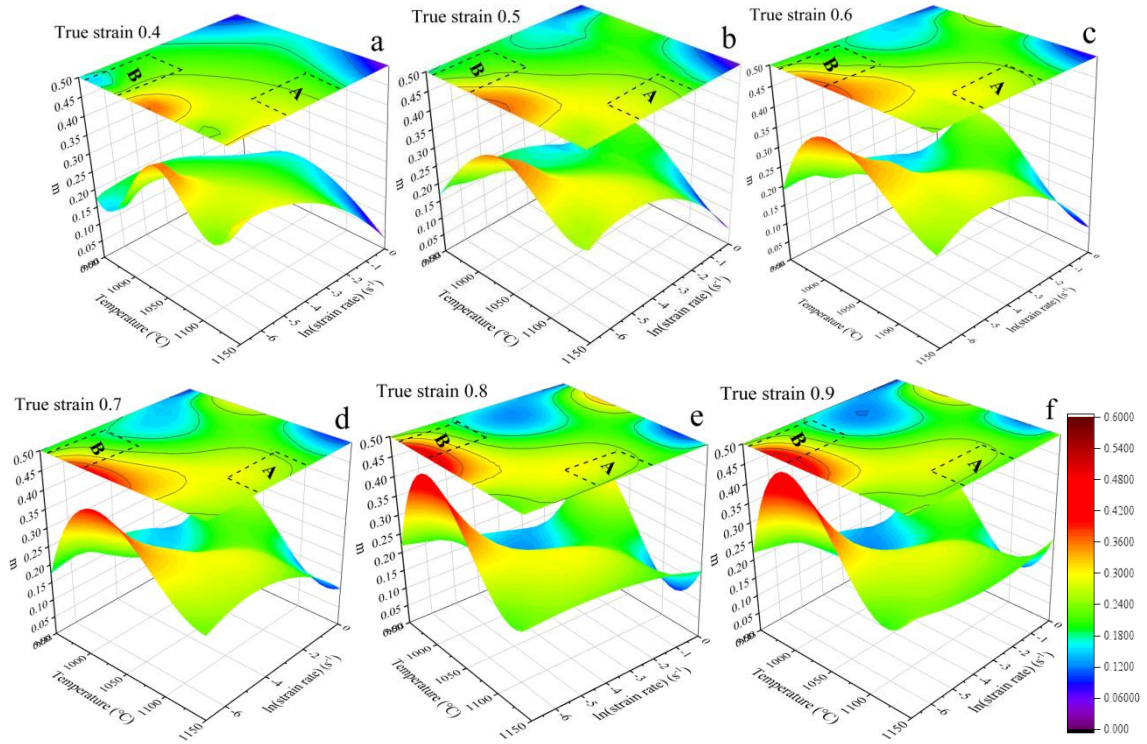


Fig. 6 The response 3D surface of  $m$ -value on temperature and strain rate at different strains of (a) 0.4, (b) 0.5, (c) 0.6, (d) 0.7, (e) 0.8, and (f) 0.9

The value of  $m$  reflects the ratio of  $J$  to  $G$ , as shown in Eqs. (2). The term  $G$  represents the power dissipated by plastic work, most of which is converted into heat, and the remaining is stored as lattice defects<sup>[10]</sup>. This indicates that the  $G$  term is a parameter related to grain coarsening or deterioration. The  $J$  term is related to the metallurgical mechanism of dynamic generation with power dissipation, which means  $J$  is the relevant parameter of grain refinement. There is a dynamic competitive relationship between  $J$  and  $G$  for refinement and coarsening, optimization and deterioration of grains. This complex mechanism shows the nonlinear relationship between strain and microstructure reconstruction efficiency with the increase of strain. Therefore, we can evaluate the competition

between  $J$  and  $G$  at a certain strain according to the value of  $m$ <sup>[8-11]</sup>. The cubic spline interpolation operation is performed on the  $m$  value, and the three-dimensional response surface maps of  $m$  to temperature and strain rate under six true strains of 0.4-0.9 were drawn, as shown in Fig. 6a-6f. It can be found that in the evolution process of  $m$ , the regions with higher value are almost located in the A-region and B-region as well as the transition position between them. With the increase of strain, the  $m$  value of B-region is increasing and is always higher than that of A-region. The change of  $m$  indicates that there are different hot deformation mechanisms<sup>[8]</sup>. At 0.4 strain, the  $m$  value in A-region is below 0.3, which is a typical feature of dislocation slip or climb-limited slip belonged to

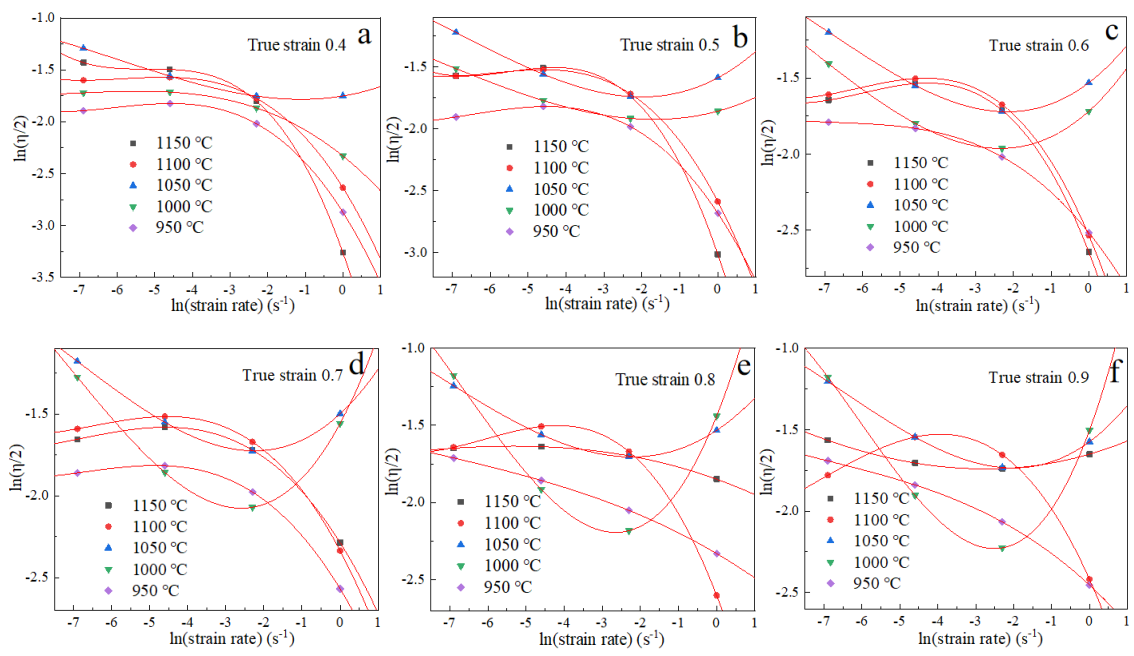


Fig. 7. The function relationship of  $\ln(\eta/2)$  and  $\ln(\text{strain rate})$  at different strains of (a) 0.4, (b) 0.5, (c) 0.6, (d) 0.7, (e) 0.8, and (f) 0.9

power-law creep mode<sup>[18]</sup>, while the  $m$  value in the center of B-region is above 0.32, which means that DRX behavior has begun<sup>[11]</sup>. As the strain continues to increase, the basal slip, non basal slip and twin plastic deformation mechanisms are coupled, making the  $m$  value continue to increase<sup>[19]</sup>. It should be noted that the power dissipation efficiency of hot working such as DRX is lower than 0.5, because power dissipation occurs through the formation of interfaces generated by dislocation rearrangement and recovery<sup>[14]</sup>. In the center of B-region, there is  $m$  value exceeding 0.5, which means there is a risk of crack initiation<sup>[10,14]</sup>. The evolution of  $m$  in A-region is always within the range of DRX mechanism, so it is the best range of temperature and strain rate for DRX behavior. According to the color distribution of  $m$ , the range of DRX mechanism reaches the maximum when the strain reaches 0.6; and the range of DRX mechanism gradually decreases when it exceeds 0.6. This conclusion can be further confirmed from the evolution of power dissipation efficiency value  $\eta$ .

### 3.5 Evolution of instability region with strain

The instability map is the response of  $\zeta$  value to temperature and strain rate at certain strain, in which the  $\zeta$  characteristic value is negative. According to Eqs. (8), The  $\zeta$  value needs to be calculated as the slope of the logarithmic curve. The logarithmic curves were obtained by polynomial fitting method, and  $\zeta$  values were calculated as the corresponding slope of experimental parameter points, as shown in Fig. 7a-7f. The cubic spline interpolation operation is carried out to plot the response maps of  $\zeta$  value to temperature and strain rate at six true strains of 0.4-0.9, as shown in Fig. 8a-8f. The unstable state and stable state regions are clarified by gray and white colors respectively.

As shown in Fig. 8a-8c, the instability region at 0.4-0.6 strain occurs at the position of high strain rate, and the instability comes from local shear or twinning, resulting in the reduction of slip<sup>[20]</sup>. When the strain exceeds 0.6, as shown in Fig. 8d-8f, instability region also appeared near B-region, and gradually increased with the strain. The instability region at

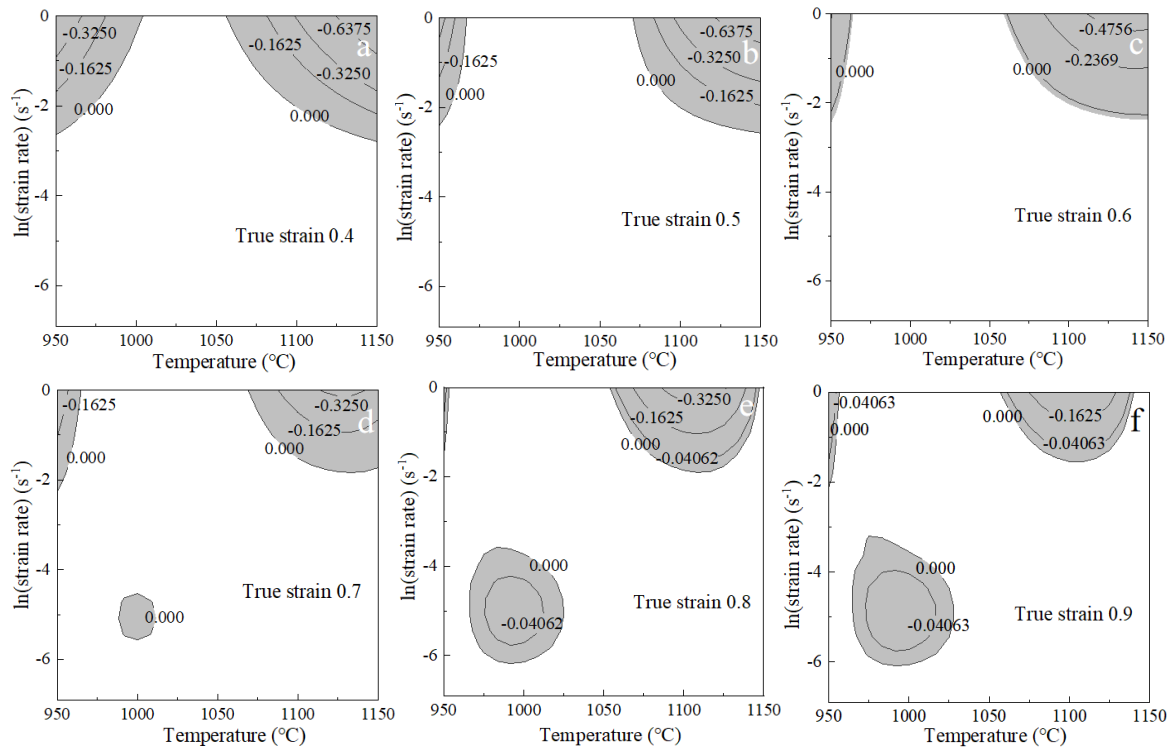


Fig. 8. The instability maps at different strains of (a) 0.4, (b) 0.5, (c) 0.6, (d) 0.7, (e) 0.8, and (f) 0.9

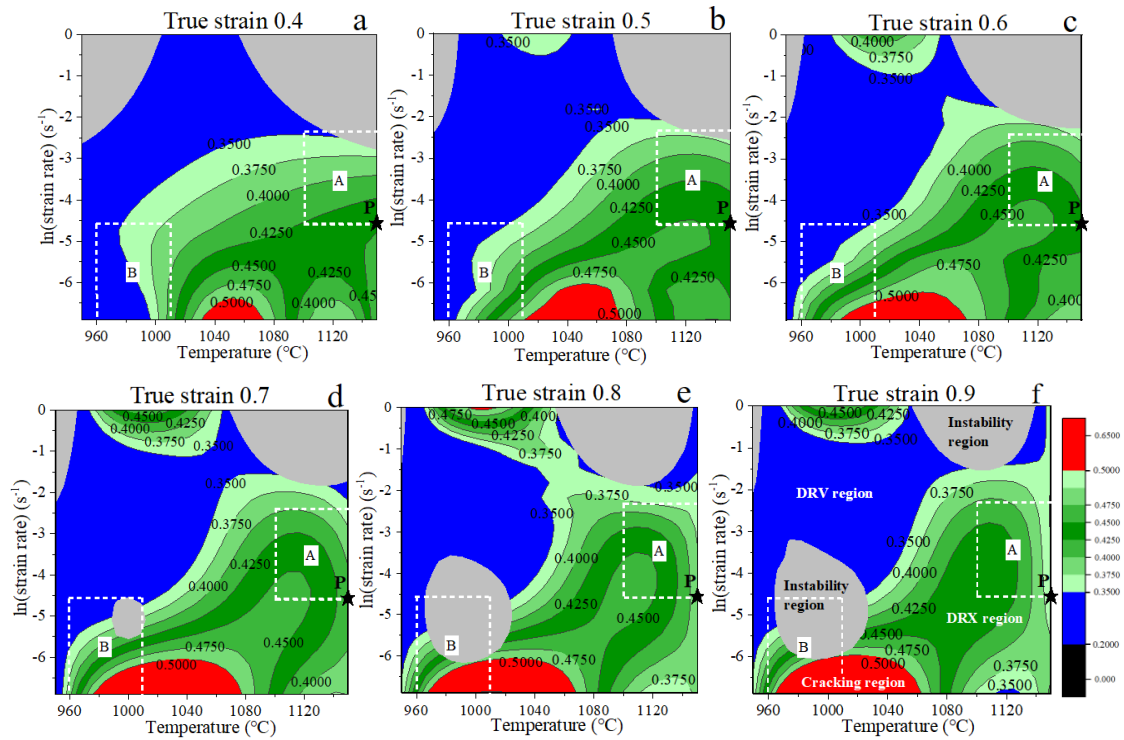


Fig. 9. The processing maps at different strains of (a) 0.4, (b) 0.5, (c) 0.6, (d) 0.7, (e) 0.8, and (f) 0.9

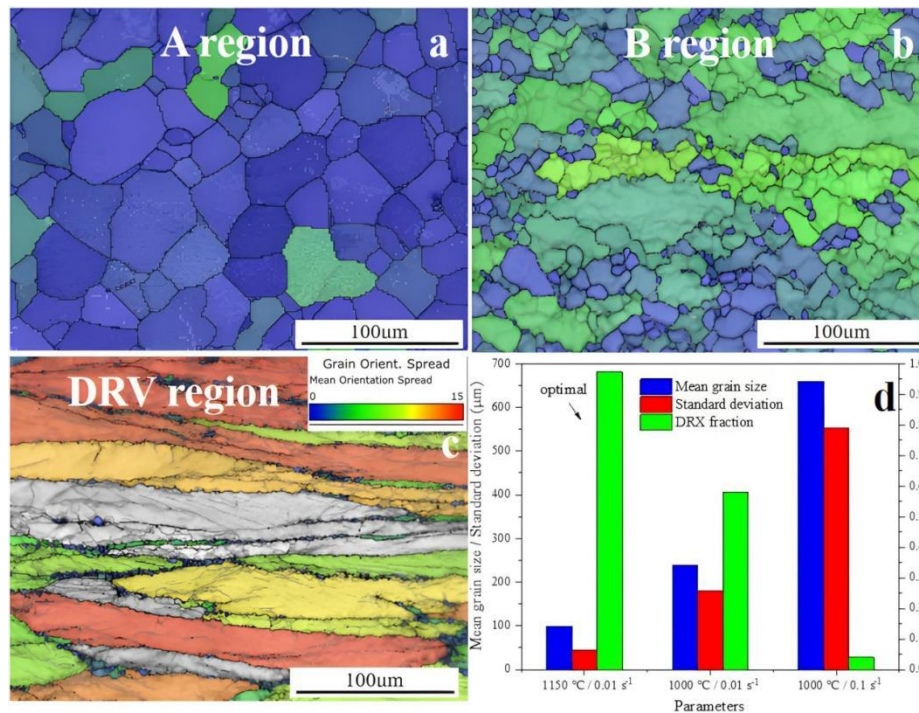
low temperature and medium strain rate generally shows coarse grain structure, which may be due to abnormal grain growth or precipitation term during deformation<sup>[14]</sup>. GH4706 alloy produces the second precipitation such as  $\text{Ni}_3\text{Ti}$  at low temperature, but it will dissolve back at high temperature. It is reported that<sup>[21]</sup> solute resistance effect will interfere with the dynamic recovery mechanism and adversely affect the formability of materials. Therefore, it can be concluded that A-region is the optimal parameter range.

### 3.6 Evolution of processing maps with strain

The processing map is the superposition of instability map and power dissipation map, which can reveal the deterministic region of metallurgical process of microstructure and the limit conditions of flow instability<sup>[7-9]</sup>. DRV and DRX are considered to be good metallurgical mechanisms, while voids, cracks, adiabatic shear bands and dynamic strain aging are considered to be bad mechanisms for microstructure deterioration<sup>[20]</sup>. Therefore, the evolution of the microstructure mechanism of the hot deformation system can be tracked by processing maps evolution at different strains. Power dissipation value  $\eta$  characterize the evolution mechanism of microstructure during hot deformation. Researches show that the  $\eta$  value of cracking process is usually very high, because the efficiency of converting power into surface energy is the highest, which is generally shown as  $\eta > 0.5$ <sup>[14]</sup>. When the power dissipation occurs with the interfaces generated by DRX and the dislocation rearrangement, the efficiency is at the medium level, which is generally shown as  $0.3 < \eta < 0.45$ <sup>[14]</sup>. Within this range, the larger the  $\eta$  value, the better the microstructure homogeniza-

tion efficiency. The  $\eta$  value is between 0.2-0.3 when the dynamic recovery behavior happens<sup>[7-9]</sup>. In addition, the efficiency peak in each region can also represent the lowest power dissipation or the highest entropy generation rate<sup>[11]</sup>.

The  $\eta$  values were calculated according to the values of  $m$ , and then were interpolated by cubic spline. The response maps of  $\eta$  to temperature and strain rate at six true strains of 0.4-0.9 were drawn, which were superimposed with the instability maps, as shown in Fig. 9a-9f. It is obvious that  $\eta$  contour shapes change at different strains. As mentioned earlier, when the  $\eta$  is less than 0.45, the larger the better. We use different shades of green color to express  $\eta$ , the darker the better. Accordingly, the optimal strain range can be approximately determined by the area contained within the 0.4 and 0.45 isolines in A-region. As shown in true strain 0.4 and 0.5 in Fig. 9a and 9b, DRX has been started in most of A-region, but a small instability area appears at the upper right corner, which will bring risk of microstructure deterioration for forgings. As the strain increases to 0.6 in Fig. 9c, A-region is all DRX area. Therefore, the microstructure of large forgings are guaranteed not to be deterioration at 0.6 strain when the parameters of each area of forging are within A-region. As shown in true strain 0.7, 0.8 and 0.9 in Fig. 9d-9f, A-region has always been the area of all DRX, but it can be found that with the increase of strain, the microstructure homogenization efficiency is decreasing, especially on the right side of A-region (the recrystallization fraction on the right side is higher). In addition, it can be found that from the strain of 0.7, instability region and cracking region appear near B-region. The method of pro-



cessing map can be used to determine the optimal strain under a certain parameter. For example, the  $\eta$  value evolution at P point (1150 °C temperature and 0.01 s<sup>-1</sup> strain rate, as asterisk mark shown in Fig. 9a-9f) shows that, the  $\eta$  value decreases from 0.45 to 0.425 as the strain increases from 0.6 to 0.7, and decreases to 0.375 as the strain increases to 0.9. Therefore, the 0.6 strain is the optimal microstructure homogenization efficiency at 1150 °C temperature and 0.01 s<sup>-1</sup> strain rate.

#### 4 Microstructure observation and verification

##### 4.1 Verification of optimal temperature region and strain rate region

The GOS maps of EBSD were used to characterize the microstructure of three regions in the processing map (A-region: 1150 °C / 0.01 s<sup>-1</sup>, B-region: 1000 °C / 0.01 s<sup>-1</sup> and DRV region: 1000 °C / 0.1 s<sup>-1</sup>) at 1.2 true strain, so as to verify the optimal parameter region, as shown in Fig. 10a-10c. The average grain size, DRX fraction and grain distribution standard deviation calculated for the three sets of parameters were shown in Fig. 10d. The microstructure of A-region in Fig. 10a shows fully recrystallized and well-developed uniform grains. However, it can be found that the grain size has grown up for a certain degree, which is caused by high temperature and low strain rate<sup>[13]</sup>. A typical imperfect recrystallization structure with some non recrystallization deformed grains can be seen in the microstructure of B-region in Fig. 10b. This verifies that B-region is also the parameter range for DRX behavior, but the microstructure homogenization efficiency is much lower

than that of A-region. The microstructure of DRV region in Fig. 10c shows non DRX structure but deformed structure. To sum up, Fig. 10 verify the correctness of using the processing map method to definite the optimal parameter range.

##### 4.2 Verification of optimal strain

The GOS maps of EBSD were used to characterize the microstructure evolution of different strains at P point (1150 °C temperature and 0.01 s<sup>-1</sup> strain rate, as shown in Fig. 9) in A-region, so as to verify the optimal strain, as shown in Fig. 11a-11f. It can be found that with the increase of strain, the microstructure grain gradually shows the trend of uniformity and refinement. This reflects the typical strain induced DRX mechanism<sup>[12]</sup>. The original microstructure has been replaced and reconstructed by DRX structure at a certain strain. The statistics of average grain size, DRX fraction and grain distribution standard deviation at different strains are shown in Fig. 11g-11i. The curves of average grain size and DRX fraction show opposite exponential evolution within 0.4-0.9 strain range, which is consistent with the typical DRX evolution characteristics<sup>[15]</sup>. It can be found in Fig. 11g-11i that after 0.6 true strain, the change rate of average grain size, DRX fraction and standard deviation tend to be obviously gentle. This means that the 0.6 true strain is at the inflection point of microstructure homogenization efficiency, which is consistent with the conclusion of the processing map and confirms the efficacy of the processing map method. This conclusion can provide a theoretical basis for the strain homogenization design of GH4706 forgings.

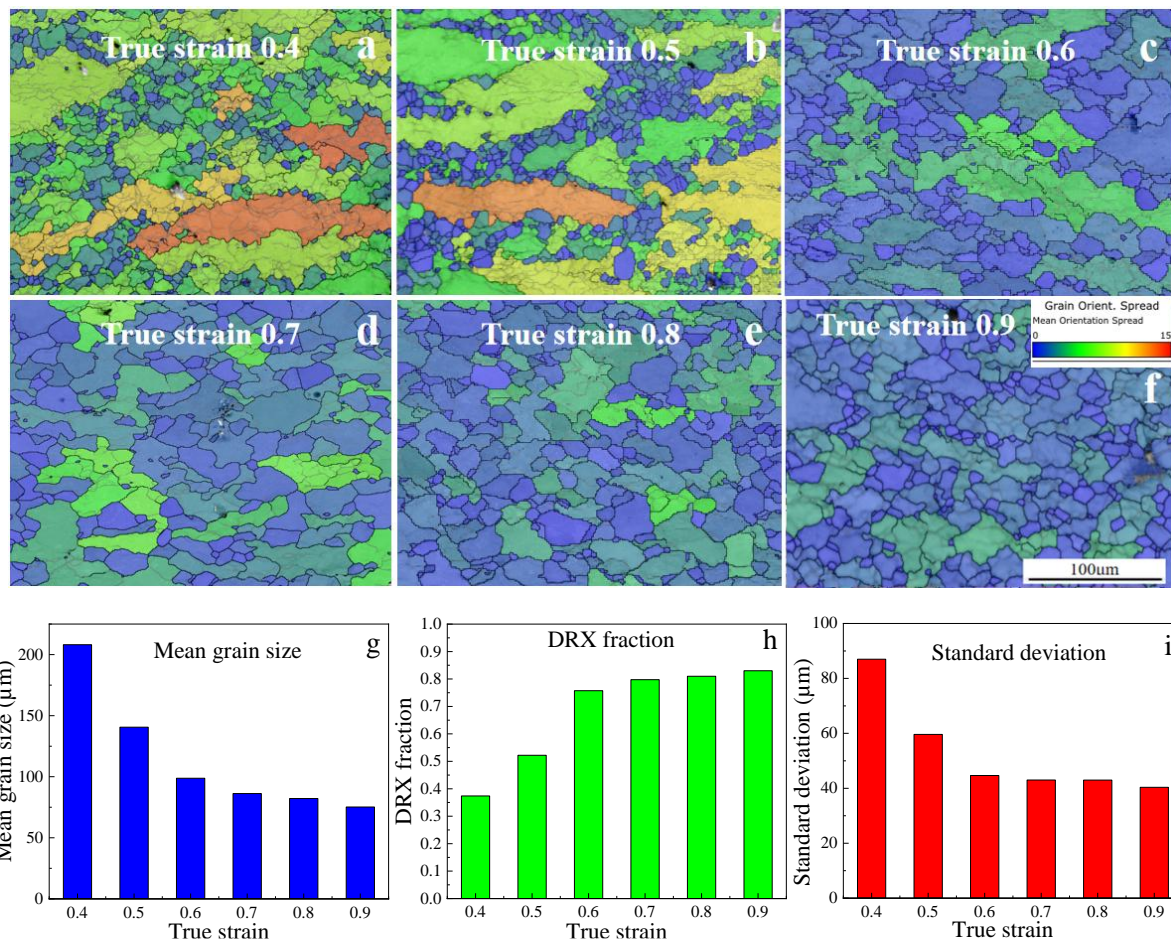


Fig.11 The GOS maps at different strains of (a) 0.4, (b) 0.5, (c) 0.6, (d) 0.7, (e) 0.8, (f) 0.9, (g) DRX fraction statistics, (h) Mean grain size statis-

## 5 Conclusion

The quantitative relationship between microstructure homogenization and process parameters of GH4706 alloy was studied by the hot deformation maps method. The main conclusions are as follows:

1. Nephogram maps of DRX fraction, average grain size, and grain distribution standard deviation at a strain of 1.2 were generated. Comprehensive analysis of these maps identified optimal parameter region A (1100-1150 °C / 0.01-0.1 s<sup>-1</sup>).

2. Processing maps at true strains ranging from 0.4 to 0.9 were developed. It was determined that the hot deformation system at a temperature of 1150 °C and a strain rate of 0.01 s<sup>-1</sup> reaches the optimal microstructure homogenization efficiency at the strain of 0.6. This method can be used to determine the optimal strain at different temperature and strain rate combinations.

3. Grain orientation spread (GOS) maps showed results consistent with the nephograms and processing maps, confirming the efficacy of the research method and results. This study provides an effective method for microstructure homogenization control of GH4706 alloy. Meanwhile, it can provide effective reference for the minimum strain threshold

of the local part of the forging in engineering.

## Reference

- [1] Sharma P, Chakradhar D, Narendranath S. *Materials and Design*[J], 2015, 88: 558
- [2] Ferro P, Zambon A, Bonollo F. *Materials Science and Engineering A*[J], 2005, 392: 94
- [3] Mukherji D, Gilles R, Barbier B *et al. Scripta Materialia*[J], 2003, 48: 143
- [4] Wang G Q, Chen M S, Li H B *et al. Journal of Materials Science & Technology*[J], 2021, 77: 47
- [5] Zhang B Y , Wang Z T, Yu H *et al. Journal of Alloys and Compounds*[J], 2022, 15: 163515
- [6] Huang S, Wang L, Lian X T *et al. International Journal of Minerals, Metallurgy and Materials*[J], 2014, 21: 462
- [7] Zheng D Y, Xia Y F, Teng H H *et al. Rare Metal Materials and Engineering*[J], 2024, 53(7): 1887
- [8] Huang S H, Zhao Z D, Xia Z X *et al. Rare Metal Materials and Engineering*[J], 2010, 39(5): 848

- [9] Zeng W D, Zhou Y G, Zhou J et al. *Rare Metal Materials and Engineering*[J], 2006, 35(5): 673
- [10] Prasad Y V, Gegel H L, Doraivelu S M et al. *Metall Trans A*[J], 1984, 15: 1883
- [11] Shen J Y, Hu L X, Sun Y et al. *Journal of Alloys and Compounds*[J], 2020, 822: 153735
- [12] Li X W, Sun H F, Zhang P et al. *Intermetallics*[J], 2014, 55: 90
- [13] Huang K, Logé R E. *Materials and Design*[J], 2016, 111: 548
- [14] Srinivasan N, Prasad Y V, Rao R P. *Materials Science and Engineering: A*[J], 2008, 476: 146
- [15] Huo Y M, Huo C L, He T et al. *Journal of Materials Engineering and Performance*[J], 2024, 33: 9893–9910
- [16] Li L, Wang Y, Li H et al. *Computational Materials Science*[J], 2019, 166: 221–229
- [17] Quan G Z, Wen Z H, Shen L et al. *Materials Reports*[J], 2021, 35: 18154
- [18] Luo J, Wang L F, Liu S F et al. *Materials Science and Engineering: A*[J], 2016, 654: 213
- [19] Quan G Z, Ku T W, Song W J et al. *Materials & Design*[J], 2011, 32: 2462
- [20] Prasad Y.V.R.K. *Journal of Materials Engineering and Performance*[J], 2003, 12: 638
- [21] Wang M J, Wang W R, Liu Z L et al. *Materials Today Communications*[J], 2018, 14: 188

## 基于热变形图方法的 GH4706 合金微观组织均匀化控制

郑德宇, 夏玉峰, 周杰

(重庆大学 材料科学与工程学院, 重庆 400044)

**摘要:** GH4706 合金在 950–1150°C 的温度范围内和 0.001–1 s<sup>-1</sup> 的应变率范围内, 在 1.2 的真实应变下进行了热压缩试验。使用动态再结晶 (DRX) 分数、平均晶粒尺寸和晶粒分布标准偏差的云图确定了最佳热变形温度和应变率范围。基于流动应力曲线绘制了 0.4 至 0.9 真实应变下的加工图, 以确定在不同温度和应变率下最佳微观组织均匀化效率相对应的应变。在最佳参数范围内, 加工图表明, 在 1150°C 和 0.01 s<sup>-1</sup> 下, 约为 0.6 的真实应变具有最高的微观组织均匀化效率。实验获得的晶粒取向扩展 (GOS) 图证明了此结论。本研究为 GH4706 合金的微观组织均匀化控制提供了一种有效的方法。同时, 它可以为工程中锻件局部最小应变阈值的确定提供有效的参考。

**关键词:** GH4706 合金; 动态再结晶; 微观组织; 均匀化效率; 加工图

作者简介: 郑德宇, 男, 1983 年生, 博士, 重庆大学 材料科学与工程学院, 重庆 400044, E-mail: [13193805@qq.com](mailto:13193805@qq.com)